

Case Report

Clinicopathologic features and exploration of new molecular mechanisms of radiation-induced bone injury: report of two cases and review of the literature

Lide Tao^{1*}, Chaowen Bai^{1*}, Xiang Gao^{1*}, Mingchao Zhang¹, Xueli Qiu¹, Yuqian Yao¹, Shuai Wei¹, Xushen Zhao¹, Lijun Wu², Xiaozhong Zhou¹, Bingchen Shan¹, Jinyu Bai¹, Huajian Shan¹

¹Department of Orthopaedics, The Second Affiliated Hospital of Soochow University, Suzhou 215004, Jiangsu, China; ²Department of Plastic and Aesthetic Surgery, The Second Affiliated Hospital of Soochow University, Suzhou 215004, Jiangsu, China. *Equal contributors.

Received November 20, 2024; Accepted January 8, 2025; Epub January 15, 2025; Published January 30, 2025

Abstract: Radiation-induced bone injury (RBI) has a multifaceted mechanism of occurrence, is influenced by various factors, and is difficult to prevent. Clinicopathologic features and manifestations of disease progression were observed in two patients with distinct fractures: one with a left-sided fourth rib fracture after postoperative radiotherapy for lung cancer, and the other with a right-sided intertrochanteric femur fracture following accidental exposure to a ¹⁹²Ir radiation source 5 years prior. These two clinical case reports discussed the clinicopathologic features of RBI and disease progression and utilized transcriptome sequencing to explore potential new targets for treating this type of RBI. Both patients exhibited similar incurable osteolytic bone destruction and fatty infiltration in their pathology. It is proposed that XIST, the most significantly upregulated gene identified by transcriptome sequencing analysis, maybe a potential target for understanding these molecular mechanisms.

Keywords: Radiation-induced bone injury, radiotherapy, ¹⁹²Ir radiation source, transcriptome sequencing

Introduction

Excessive doses of ionizing radiation can lead to metabolic and clinicopathological changes in bone tissue, resulting in decreased bone strength and an increased risk of fracture; this is known as radiation-induced bone injury (RBI) [1, 2]. Pathological changes in the bone can be categorized as radiation osteoporosis, osteoradionecrosis, radiation pathologic fracture, osteoradionecrosis, and radiation dysostosis [3]. RBI typically occurs as a complication of clinical radiotherapy or in the event of nuclear accidents, with the high calcium content of bone allowing it to absorb more than 30%-40% more radiation than surrounding tissues [4]. Radiation can directly impact bone-associated cells [5-7], leading to alterations in bone morphology and an increased risk of bone loss and fractures. Furthermore, radiation can damage the microstructure and mechanical properties of bone by disrupting its mineral and organic components [8, 9]. A previous study showed

that patients with anal, cervical, and rectal cancers face a greater risk of pelvic fracture by 216%, 66%, and 65%, respectively, following pelvic radiotherapy [10]. The exact molecular mechanism underlying the pathological changes in RBI remains unclear, and effective preventive and therapeutic measures are lacking [11]. Further research is needed to explore new molecular mechanisms and prevention strategies for RBI.

We present case reports of RBI caused by radiotherapy and exposure to an Iridium-192 (¹⁹²Ir) radiation source, along with an analysis of RNA-seq results from an animal model. We aimed to offer insights for early intervention in the development of RBI.

Case presentation

Patient 1

A 58-year-old male patient was admitted to the Department of Thoracic Surgery at our hospital,

Features and mechanisms of radiation-induced bone injury

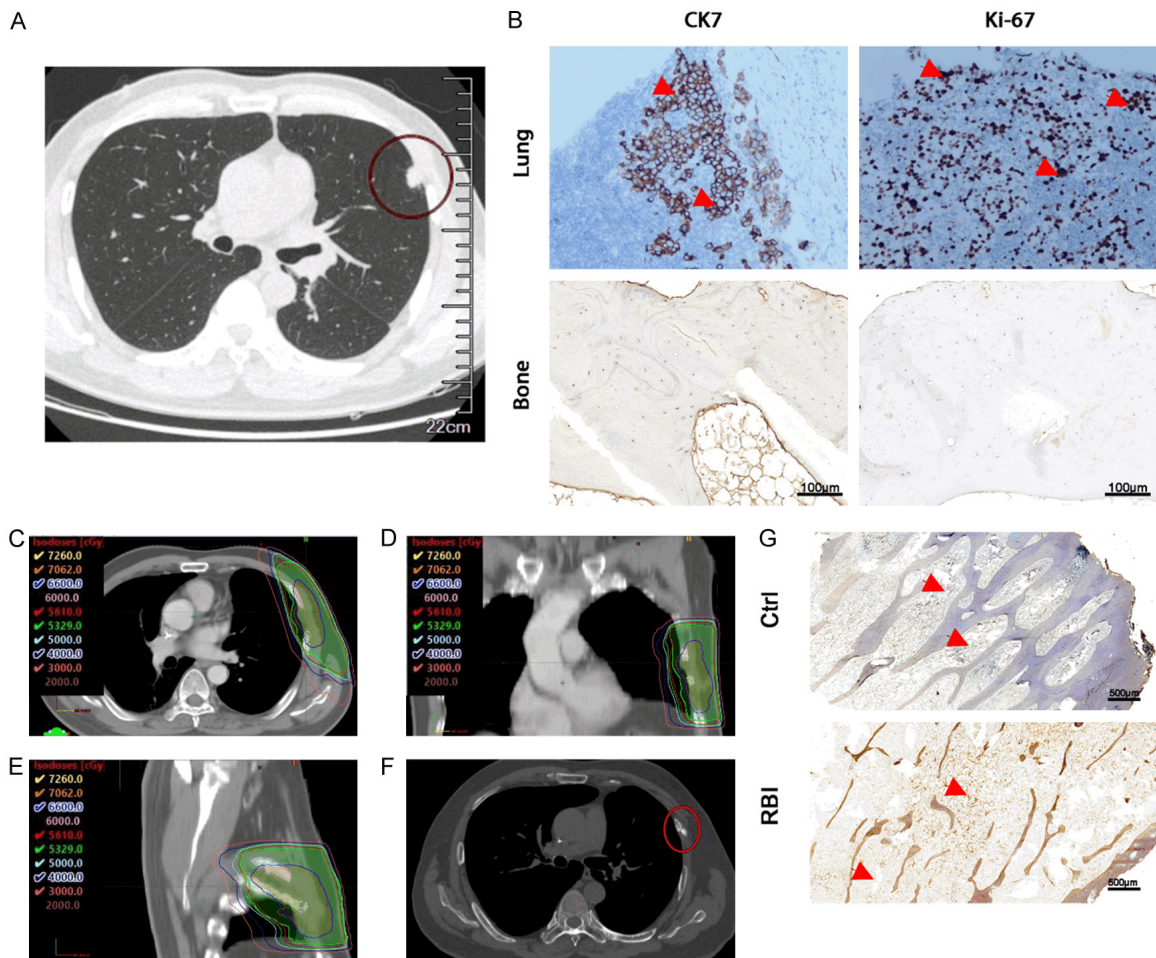


Figure 1. Detailed progression of lesions for patient 1 before and after radiotherapy. A. The CT scan reveals a subpleural mass shadow located in the lingual segment of the left upper lobe. This mass is closely adherent to the pleura and predominantly consists of a lobulated solid component featuring distinct burr-like projections. B. Immunohistochemistry of lung tissue showed CK7 (+) and Ki-67 (+, 70%), while immunohistochemistry of rib tissue showed CK (-), and Ki 67 (-). C-E. The postoperative radiotherapy plan demonstrates a coverage window with a prescription dose of PGTV of 6600 cGy/220 cGy/30 frequency. F. A CT scan revealed cortical discontinuity of the fourth rib on the left side. G. RBI bone tissue sections of the ribs in more unirradiated areas displayed extensive destruction of bone trabeculae, replaced by adipocytes (arrows), with no infiltration of cancer cells observed.

where he underwent radical pulmonary resection surgery. This procedure was necessitated by the identification of a malignant nodule in the left upper lung during computed tomography (CT) health screening (Figure 1A). Post-operative pathology revealed poorly differentiated adenocarcinoma of the left upper lung, with immunohistochemistry results showing CK7 (+) and Ki-67 (+, 70%) (Figure 1B). Due to manifestations of intolerance, including vomiting, loss of appetite, and leukopenia, observed after several postoperative administrations of the chemotherapeutic agents carboplatin and paclitaxel, a localized radiation therapy regimen was conducted over a nine-month period,

delivering a total dose of 66 Gy (Figure 1C-E), two years following the surgery. A recurrent complication of chest ulcers with associated pain was observed during radiotherapy. The patient presented to our hospital 5 months after completing radiotherapy, and a cortical discontinuity of the left fourth rib was identified on a CT scan (Figure 1F). Subsequently, partial resection of the fourth rib and flap transfer repair were performed. Paraffin sectioning of the resected rib revealed a decrease in bone tissue minerals, thinning of the bone structure, a decrease in bone trabeculae, and the substitution of bone marrow with fibrous tissue and lymphocytes relative to those in unirradiated

ribs (**Figure 1G**). Immunohistochemistry results indicated no signs of cancer cell metastasis in the bone tissue, with CK7 (-) and Ki-67 (-) findings (**Figure 1B**).

Patient 2

A 62-year-old male patient presented to our hospital 5 days after an accidental exposure to a ^{192}Ir radiation source, leading to right extremity skin ulceration. The investigation revealed that the radiation source had an activity of 25 Ci, roughly the size of a soybean. Upon evaluation, it was determined that the estimated whole-body irradiation dose was 1.41 Gy, with the right lower extremity receiving a local average dose of 36 Gy. Patients with mild bone marrow form of acute radiation sickness (BM-ARS) resulting from external irradiation are managed with supportive and anti-infective therapy, transitioning to the recovery phase 40 days postirradiation. After 1 month of the exposure, a noticeably greater percentage of mature monocytes were observed on the right side of the bone marrow smear than on the left side (**Figure 2A, 2B**). The patient underwent multiple right lower limb flap transplantations and received anti-infective treatment for radiation-induced skin damage. Following improvement, the patient was transferred to a rehabilitation hospital for ongoing treatment to enhance functional recovery of the right lower limb. Subsequently, regular medical follow-up was conducted, revealing a progressive increase in abnormal signals in the right femur on magnetic resonance imaging (MRI) (**Figure 2C-F**) and bone turnover markers (**Figure 2I**). Five years later, the patient presented with pain and limited mobility in the right lower limb during physical activity. He sought treatment at our hospital, where an MRI revealed an intertrochanteric fracture and osteoradiomyelitis of the lower part of the right femur (**Figure 2F**). Subsequently, the patient underwent external fixation bracket placement for the right femur fracture (**Figure 2G, 2H**). Intraoperative pathological findings indicated necrotic trabecular bone, and abundant fat vacuoles (**Figure 2J**).

Exploration of potential molecular mechanisms of RBI

RBI model in mice

To further elucidate the molecular mechanisms of RBI, transcriptome sequencing assays were

conducted on the mRNAs of both the experimental and control groups in an animal model. C57BL/6J mice, females, 4 months old, were purchased from Shanghai SLAC Laboratory Animal Co., Ltd. (Shanghai, China). The femurs of mice in the experimental group were irradiated locally with an 80 cGy dose of intermittent radiation 10 times, and cell samples were collected 10 weeks later to establish an optimal model of RBI [12]. The success of model construction can be efficiently assessed by observing significant bone destruction, which includes trabecular changes and a reduction in cellular density [13]. Mice were maintained under specific pathogen-free animal research facilities, with a 12-hour dark/12-hour light cycle, $22^{\circ}\text{C} \pm 1^{\circ}\text{C}$ temperatures, and ad libitum access to food.

Library preparation and sequencing

RNA purification, reverse transcription, library construction, and sequencing were conducted at Shanghai Majorbio Bio-pharm Biotechnology Co., Ltd. The preparation of the RNA-seq transcriptome library was carried out in accordance with the Illumina Stranded mRNA Prep, Ligation protocol (San Diego, CA), utilizing 1 μg of total RNA as the starting material. Initially, messenger RNA was isolated through a polyA selection method using oligo(dT) beads, and this was followed by fragmentation using fragmentation buffer. Subsequently, double-stranded complementary DNA (cDNA) was synthesized with the aid of a SuperScript double-stranded cDNA synthesis kit (Invitrogen, CA) employing random hexamer primers during the synthesis process. The produced cDNA underwent several steps in preparation for the final library, including end-repair, phosphorylation, and the incorporation of adapters, all performed in line with the established library construction protocol. To ensure the proper size of the cDNA target fragments, the libraries underwent size selection on 2% Low Range Ultra Agarose to specifically isolate fragments of approximately 300 base pairs. These selected fragments were then amplified through PCR using Phusion DNA polymerase for a total of 15 PCR cycles. Finally, after quantification using the Qubit 4.0 system, the sequencing library was prepared for sequencing on the NovaSeq X Plus platform, utilizing the NovaSeq Reagent Kit for effective sequencing processes.

Features and mechanisms of radiation-induced bone injury

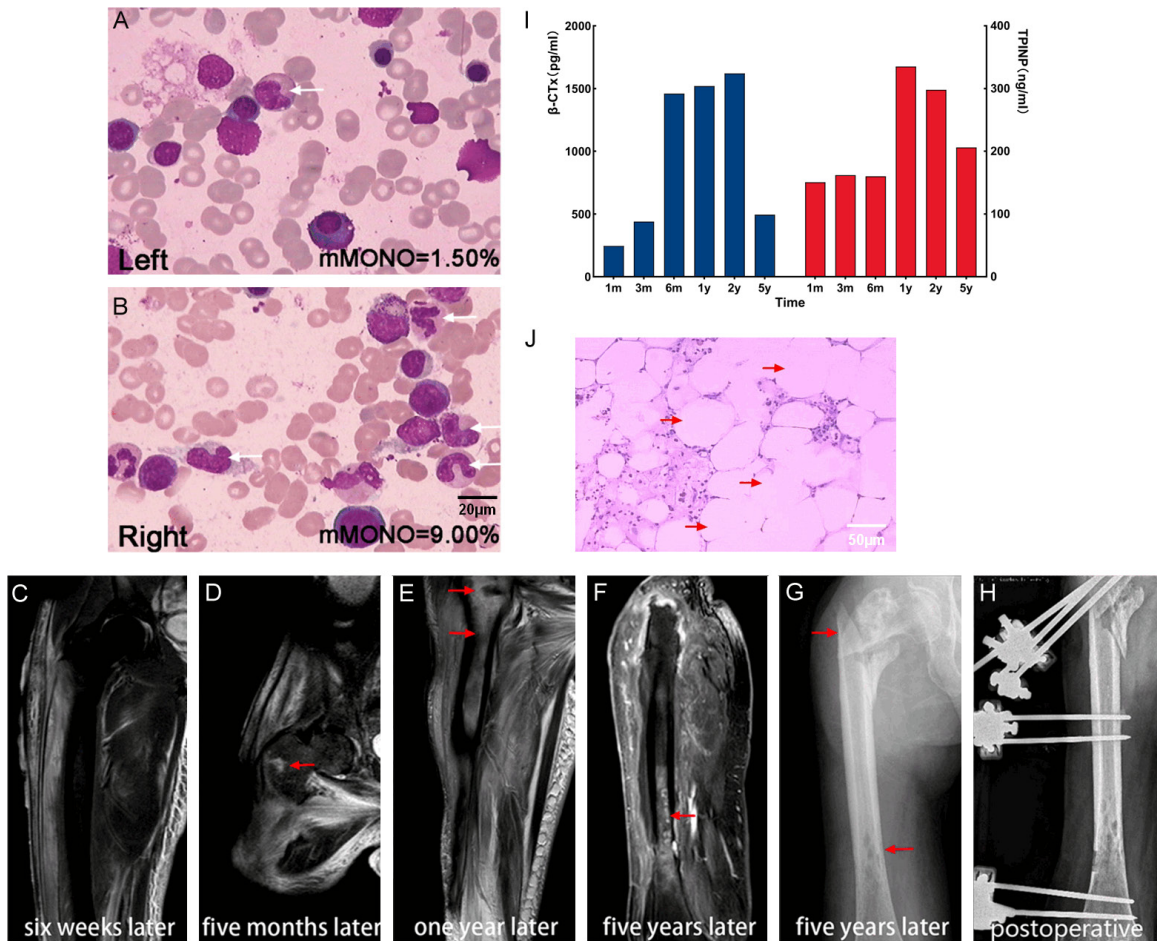


Figure 2. Detailed lesions in patient 2 after exposure to ^{192}Ir radiation source. A and B. One month later, there was a notable increase in the number of mature monocytes in the right lower extremity compared to the left extremity (arrows). The percentage of mature monocytes in the bone marrow smear of the left lower extremity was 1.50%, while in the right lower extremity it was 9.00%. C-G. RBI image of the ^{192}Ir source accident involving the right femur. C. Six weeks later, T2WI-SPAIR revealed large soft tissue abnormal signals with no bone marrow cavity abnormalities. D. Five months later, T2WI-SPAIR showed flaky edema signals in the bone marrow cavity of the upper segment of the right femur. E. One year later, there were significantly more abnormal signals in the upper segment of the femur than in the previous segment. F. Five years later, the enhanced NMR signal displayed multiple small nodular low-signal foci in the middle and lower segments of the right femur with uneven enhancement. G. Proximal bone fracture and irregular bone cortex thinning were observed (arrows). H. Postoperative internal fixation of the fracture was performed. I. The bone turnover markers $\beta\text{-CTx}$ and TPINP were significantly increased and peaked at 1-2 years. J. Intraoperative biopsy revealed necrotic trabecular bone, collagen fibers, and abundant fat vacuoles (arrows).

Differential expression analysis and functional enrichment

To determine differentially expressed genes (DEGs) between two distinct samples, the expression levels of each transcript were computed using the transcripts per million reads (TPM) approach. Differential expression analysis was essentially conducted utilizing DESeq2 [14]. Genes that exhibited $|\log_2\text{FC}| \geq 1$ and $\text{FDR} < 0.05$ were classified as significantly differently expressed. Furthermore, a functional

enrichment analysis, which included KEGG, was conducted to ascertain which DEGs were notably enriched in metabolic pathways, with Bonferroni-corrected P -values of less than 0.05 in relation to the entire transcriptome background. KEGG pathway analysis was performed using Python's scipy software.

Results of the RNA-seq

Analysis of the RNA-seq data revealed 490 genes with upregulated expression and 407

Features and mechanisms of radiation-induced bone injury

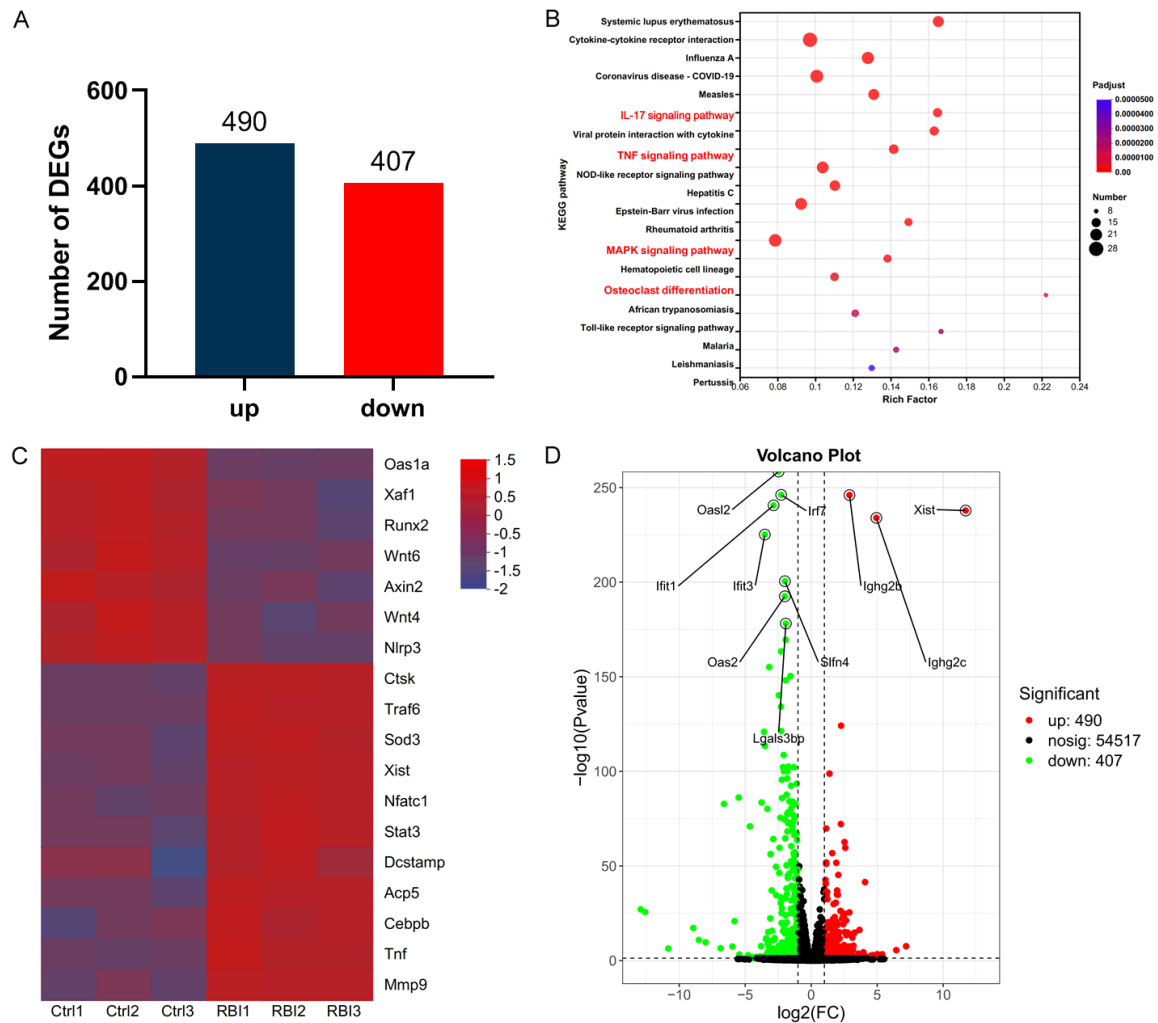


Figure 3. Analysis of differentially expressed genes from RNA-seq. **A.** The RNA-seq results were analyzed for DEGs. Upregulated genes are represented by blue while downregulated genes are indicated by red. A total of 490 genes were upregulated and 407 genes were downregulated. **B.** KEGG pathway enrichment revealed that the DEGs were associated with signaling pathways, primarily involving the IL-17, TNF, MAPK, and osteoclast differentiation pathways. **C.** Heatmap illustrates the up-regulation of osteoclast-related gene (CTSK, TRAF6, NFATC1 et al.) expression and the down-regulation of genes osteoblast-related gene (Runx2, Wnt, Axin et al.) expression in the RBI group of mice. **D.** The volcano plot of DEGs highlighted the 10 genes with the most significant differences.

genes with downregulated expression (**Figure 3A**). KEGG pathway enrichment analysis of these differentially expressed genes highlighted signaling pathways such as apoptosis, the MAPK cascade, and osteoclast differentiation (**Figure 3B**). In the RBI animal model, we observed that genes associated with osteoclast function and lipogenesis were upregulated, whereas genes related to osteoblast were downregulated (**Figure 3C**). Following irradiation, genes of research interest were identified, with IGHG2 and XIST showing the most significant upregulation and OASL, IFIT and IRF

being the most noticeably downregulated (**Figure 3D**).

Discussion

The incidence of localized rib injuries following radiotherapy in breast cancer patients ranges from 0.4% to 5.7% [15, 16], and there is a lack of specific descriptions in the literature regarding rib fractures and injuries resulting from ¹⁹²Ir radiation sources post-radiotherapy. As such, we have compiled an overview of the pathology and imaging patterns associated with RBI. This case report details the clinicopathologic fea-

Features and mechanisms of radiation-induced bone injury

tures and imaging manifestations of a radiotherapy-induced rib fracture and a rare hip fracture caused by a ^{192}Ir radiation source, along with BM-ARS and osteoradiomyelitis.

One of the tissues sensitive to radiation is the bone marrow, where a dose of 1-10 Gy can cause BM-ARS [17], which can be reversible and depends on several additional situations. This condition is characterized by a decrease in peripheral whole blood cells, and hematopoietic stem cells, and can lead to complications such as infections and bleeding [18]. The effects of radiation on myeloid cells are first observed in peripheral blood cells. Hence, the early analysis of bone marrow smears is important. In the second case study, the patient's bone marrow smear at 4 weeks revealed a low granulocyte-to-erythrocyte (G/E) ratio of 1.24:1 and a high monocyte percentage of 9.00%. These findings may be associated with osteoclast activation [19], which gradually improved following anti-infective treatment. Following radiation exposure, the most significant decrease in lymphocytes occurs within 6-24 hours [20], followed by decreases in neutrophils and platelets [21]. Currently, treatment options for BM-ARS are limited, emphasizing the urgent need for the development of drugs for the prevention, mitigation, and treatment of BM-ARS.

Distinguishing RBI from rib metastasis in lung cancer patients is crucial in clinical practice. RBI typically presents with bone destruction within the radiation field, manifesting as patchy worm-eaten changes. This condition is often associated with radiation pneumonitis in the corresponding area, a lack of soft tissue masses, and the presence of thickened and broken skin within the radiation field. Over time, radiological rib injury may show signs of spontaneous healing or remain stable without significant changes during follow-up. Lung cancer bone metastasis is primarily driven by hematogenous spread, leading to bone resorption by osteoclasts and the formation of osteolytic lesions [22]. Upon metastasis to bone, lung cancer cells release signaling molecules that trigger the activation of osteoclasts and osteoblasts. The cytokines released by osteoclasts further stimulate tumor cells to produce osteolytic factors, creating a detrimental feedback loop. Treatment with osteoclast-inhibiting drugs, such as bisphosphonates, can effectively

reduce osteoclast activity in malignant bone lesions, thereby mitigating hypercalcemia and hyperuricemia [23].

The case of osteoradiomyelitis may have been caused by a secondary infection following localized immune deficiency due to RBI. Osteoradiomyelitis presents a complex imaging profile and must be distinguished from other forms of osteomyelitis [24]. Patients with acute osteomyelitis typically exhibit soft-tissue swelling in the early stages, followed by extensive bone destruction in the medullary cavity, early subperiosteal abscess formation, mild periosteal reaction, and dead bone formation [25]. Chronic osteomyelitis is characterized by evident bone hyperplasia surrounding bone destruction, clear periosteal reaction, dead bone, and sinus tracts. Sclerosing osteomyelitis presents with localized symptoms, evident bone hyperplasia sclerosis, cortical thickening, and narrowing and occlusion of the medullary cavity [26, 27]. In this case, the patient's MRI primarily revealed bone destruction, irregular thinning of the bone cortex, subperiosteal fluid collection, infection in the medullary cavity, soft tissue swelling with infection, and sinus tract formation, indicative of osteoradiomyelitis.

The mechanism of RBI is intricate, and influenced by multiple factors, posing challenges for prevention. Current understanding points to vascular damage and disruption of the osteogenic-osteoclastic balance as primary mechanisms [9, 28], yet their precise molecular pathways remain elusive. Exploring new potential therapeutic drugs and treatment methods is essential for addressing RBI. Identifying characteristic genes or molecules linked to RBI could be used as indicators for predicting and treating such damage [29]. Total mRNA was extracted for high-throughput sequencing from the groups of experimental and control model mice. Differential gene expression analysis was then conducted on the sequencing data. The most significant upregulation of the XIST gene, known for its important role in mammalian X chromosome inactivation by targeting specific autosomal regions and inducing repressive chromatin changes, may mediate immune regulation [30-32]. Further investigation and additional experimental and clinical data are required to confirm whether the most significant XIST gene upregulation contributes to RBI

Features and mechanisms of radiation-induced bone injury

and elucidate the exact underlying mechanism.

Acknowledgements

This work was supported by the National Natural Science Foundation of China (Nos. 82472515, 82402826); the Gusu health talent plan-special talents C (2021) 021, (2022) 009; the Gusu health talent plan-research project (GSWS2021015, GSWS2022038); China National Nuclear Corporation Young talent project; and Jiangsu Provincial Health Commission Guiding project (Z2022010).

All patients provided informed consent for publication of this case report and accompanying images.

Disclosure of conflict of interest

None.

Abbreviations

¹⁹²Ir, Iridium-192; BM-ARS, bone marrow form of acute radiation sickness; CT, computed tomography; DEGs, differentially expressed genes; KEGG, Kyoto Encyclopedia of Genes and Genomes; NMR, Nuclear magnetic resonance; PGTV, planning gross tumor volume; RBI, radiation-induced bone injury; T2WI-SPAIR, T2 weighted image-Spectral Attenuated Inversion Recovery.

Address correspondence to: Huajian Shan, Jinyu Bai and Bingchen Shan, Department of Orthopaedics, The Second Affiliated Hospital of Soochow University, Suzhou 215004, Jiangsu, China. Tel: +86-15162244048; E-mail: shanhj@suda.edu.cn (HJS); Tel: +86-15365301155; E-mail: baijy@suda.edu.cn (JYB); Tel: +86-13771960770; E-mail: shan_bingchen@163.com (BCS)

References

- [1] Willey JS, Lloyd SA, Nelson GA and Bateman TA. Space radiation and bone loss. *Gravit Space Biol Bull* 2011; 25: 14-21.
- [2] Willey JS, Lloyd SA, Nelson GA and Bateman TA. Ionizing radiation and bone loss: space exploration and clinical therapy applications. *Clin Rev Bone Miner Metab* 2011; 9: 54-62.
- [3] Williams HJ and Davies AM. The effect of X-rays on bone: a pictorial review. *Eur Radiol* 2006; 16: 619-633.
- [4] Costa S and Reagan MR. Therapeutic irradiation: consequences for bone and bone marrow adipose tissue. *Front Endocrinol (Lausanne)* 2019; 10: 587.
- [5] Celii FG and Beckmann NM. Radiation-induced insufficiency fracture of the femur 18 years after radiation therapy. *Radiol Case Rep* 2018; 14: 179-183.
- [6] Omolehinwa TT and Akintoye SO. Chemical and radiation-associated jaw lesions. *Dent Clin North Am* 2016; 60: 265-277.
- [7] Hopewell JW, Nyman J and Turesson I. Time factor for acute tissue reactions following fractionated irradiation: a balance between repopulation and enhanced radiosensitivity. *Int J Radiat Biol* 2003; 79: 513-524.
- [8] Gong B, Oest ME, Mann KA, Damron TA and Morris MD. Raman spectroscopy demonstrates prolonged alteration of bone chemical composition following extremity localized irradiation. *Bone* 2013; 57: 252-258.
- [9] Wright LE, Buijs JT, Kim HS, Coats LE, Scheidler AM, John SK, She Y, Murthy S, Ma N, Chin-Sinex HJ, Bellido TM, Bateman TA, Mendonca MS, Mohammad KS and Guise TA. Single-limb irradiation induces local and systemic bone loss in a murine model. *J Bone Miner Res* 2015; 30: 1268-1279.
- [10] Baxter NN, Habermann EB, Tepper JE, Durham SB and Virnig BA. Risk of pelvic fractures in older women following pelvic irradiation. *JAMA* 2005; 294: 2587-2593.
- [11] Somay E, Yilmaz B, Topkan E, Kucuk A, Pehlivan B and Selek U. Assessment of the impact of osteoradionecrosis on quality-of-life measures in patients with head and neck cancer. In: Sergi CM, editors. *Advancements in Cancer Research*. Brisbane (AU): Exon Publications Copyright: The Authors.; The authors confirm that the materials included in this chapter do not violate copyright laws. Where relevant, appropriate permissions have been obtained from the original copyright holder(s), and all original sources have been appropriately acknowledged or referenced.; 2023.
- [12] Emerzian SR, Wu T, Vaidya R, Tang SY, Abergel RJ and Keaveny TM. Relative effects of radiation-induced changes in bone mass, structure, and tissue material on vertebral strength in a rat model. *J Bone Miner Res* 2023; 38: 1032-1042.
- [13] Xu J, Zheng Z, Fang D, Gao R, Liu Y, Fan ZP, Zhang CM and Wang SL. Early-stage pathogenic sequence of jaw osteoradionecrosis in vivo. *J Dent Res* 2012; 91: 702-708.
- [14] Love MI, Huber W and Anders S. Moderated estimation of fold change and dispersion for RNA-seq data with DESeq2. *Genome Biol* 2014; 15: 550.

Features and mechanisms of radiation-induced bone injury

- [15] Pierce SM, Recht A, Lingos TI, Abner A, Vicini F, Silver B, Herzog A and Harris JR. Long-term radiation complications following conservative surgery (CS) and radiation therapy (RT) in patients with early stage breast cancer. *Int J Radiat Oncol Biol Phys* 1992; 23: 915-923.
- [16] Boyages J, Bosch C, Langlands AO, Bilous AM, Barraclough B and Gebiski VJ. Breast conservation: long-term Australian data. *Int J Radiat Oncol Biol Phys* 1992; 24: 253-260.
- [17] Talapko J, Talapko D, Katalinić D, Kotris I, Erić I, Belić D, Vasilj Mihaljević M, Vasilj A, Erić S, Flam J, Bekić S, Matić S and Škrlec I. Health effects of ionizing radiation on the human body. *Medicina (Kaunas)* 2024; 60: 653.
- [18] Singh VK and Seed TM. A review of radiation countermeasures focusing on injury-specific medicinals and regulatory approval status: part I. Radiation sub-syndromes, animal models and FDA-approved countermeasures. *Int J Radiat Biol* 2017; 93: 851-869.
- [19] Kubatzky KF, Uhle F and Eigenbrod T. From macrophage to osteoclast - How metabolism determines function and activity. *Cytokine* 2018; 112: 102-115.
- [20] Dainiak N, Waselenko JK, Armitage JO, MacVittie TJ and Farese AM. The hematologist and radiation casualties. *Hematology Am Soc Hematol Educ Program* 2003; 2003: 473-496.
- [21] Dainiak N. Hematologic consequences of exposure to ionizing radiation. *Exp Hematol* 2002; 30: 513-528.
- [22] Wang W, Shen K, Liu R and Zhou Q. Sema3A inhibits osteolytic bone metastasis of non-small cell lung cancer. *Recent Pat Anticancer Drug Discov* 2024; [Epub ahead of print].
- [23] O'Carrigan B, Wong MH, Willson ML, Stockler MR, Pavlakis N and Goodwin A. Bisphosphonates and other bone agents for breast cancer. *Cochrane Database Syst Rev* 2017; 10: CD003474.
- [24] Tsur N, Segal E, Kurman N, Tzelnick S, Wiesel O, Wilk L, Hamzany Y, Bachar G and Shoffel-Havakuk H. Post-radiotherapy osteomyelitis of the cervical spine in head and neck cancer patients. *BJR Open* 2023; 5: 20230001.
- [25] Capponi M, Pires Marafon D, Rivosecchi F, Zhao Y, Pardeo M, Messia V, Tanturri de Horatio L, Tomà P, De Benedetti F and Insalaco A. Assessment of disease activity using a whole-body MRI derived radiological activity index in chronic nonbacterial osteomyelitis. *Pediatr Rheumatol Online J* 2021; 19: 123.
- [26] Lee YJ, Sadigh S, Mankad K, Kapse N and Rajeswaran G. The imaging of osteomyelitis. *Quant Imaging Med Surg* 2016; 6: 184-198.
- [27] Jennin F, Bousson V, Parlier C, Jomaah N, Khanine V and Laredo JD. Bony sequestrum: a radiologic review. *Skeletal Radiol* 2011; 40: 963-975.
- [28] Pacheco R and Stock H. Effects of radiation on bone. *Curr Osteoporos Rep* 2013; 11: 299-304.
- [29] Schenone M, Dančik V, Wagner BK and Clemens PA. Target identification and mechanism of action in chemical biology and drug discovery. *Nat Chem Biol* 2013; 9: 232-240.
- [30] Brockdorff N, Bowness JS and Wei G. Progress toward understanding chromosome silencing by Xist RNA. *Genes Dev* 2020; 34: 733-744.
- [31] Dror I, Chitiashvili T, Tan SYX, Cano CT, Sahakyan A, Markaki Y, Chronis C, Collier AJ, Deng W, Liang G, Sun Y, Afasizheva A, Miller J, Xiao W, Black DL, Ding F and Plath K. XIST directly regulates X-linked and autosomal genes in naive human pluripotent cells. *Cell* 2024; 187: 110-129, e131.
- [32] Gupta K, Czerminski JT and Lawrence JB. Trisomy silencing by XIST: translational prospects and challenges. *Hum Genet* 2024; 143: 843-855.